Adaptive Charge Estimation of Piezoelectric Actuators with a Variable Sensing Resistor, an Artificial Intelligence Approach

Morteza Mohammadzaheri*, Hamidreza Ziaiefar, Mojtaba Ghodsi,
Mohammadreza Emadi, Musaab Zarog, Payam Soltani and Issam Bahadur

Abstract— Experiments have shown that, for an extensive area of operating, charge of a piezoelectric actuator is proportional to its displacement from relaxing state. Consequently, accurate estimation of charge can lead to position/displacement estimation for piezoelectric actuators, a prominent progress towards precise sensorless micro/nanopositioning. However, disadvantageously, all known charge estimators of piezoelectric actuators have electrical element(s), e.g. (a) resistor(s) or (a) capacitor(s), in series with the actuator. Such elements, known as sensing elements, take a considerable share of the excitation voltage. Voltage taken by the sensing elements is called voltage drop. Charge estimators with a resistor in series with the actuator (also known as digital charge estimators) have been reported to witness the smallest voltage drop. The aim of this paper is to design such charge estimators so as to achieve maximum precision at minimum possible voltage drop. The aforementioned aim is shown to be obtained when the range of the voltage across the resistor equals the narrowest input range of the analogue to digital convertor of the charge estimator. This, however, is impossible to happen for wide operating areas with a sensing resistor with unchangeable resistance, according to experimental results. The alternative is an adaptive charge estimator with a resistor, in which its resistance varies with operating conditions. This paper presents two methods to estimate such a varying sensing resistor: approximate analytical formulation and artificial intelligence, in which, the latter shows evident superiority.

Index Terms— Piezoelectric Actuator, Charge, Fully Connected Cascade Network, Voltage Drop, Precision.

I. INTRODUCTION

Nanopositioning is a major part of nanotechnology, targeting precise motion control at nanometre scale. Biological cell manipulation [1], scanning probe microscopy [2] [3], ultra-fine machining [4] and robotic surgery [5] are just some examples of applications benefit vastly from nanopositioning. A variety of actuators have been employed for nano/micropositioning such as magnetostrictive actuators [6], worm gears [7] and linear motors [8]. Amid all, piezoelectric actuators are the most precise and the least bulky ones [9]. They are now the most commonly used actuators in nanopositioning and seem to sustain this popularity for years [10].

The major task in piezo-actuated nanopositioning is accurate position control of (an unfixed point/surface of) the actuator [11]. The origin of (a point/surface) position is the location (of the same point/surface) at relaxing state, when the actuator has not been excited for a reasonably long time (e.g. some minutes). Experiments have demonstrated that charge of a piezoelectric actuator is proportional to its position for an extensive operating area [12-15]. That is, a charge estimator can replace a relatively costly and troublesome displacement/position sensor. This has been the main motivation behind design of charge estimators for piezoelectric actuators [9, 16, 17].

All reported charge estimators consist of electrical element(s) (e.g. capacitor(s) or resistor(s)) in series with the piezoelectric actuator [18]. These elements are named sensing elements. The voltage across the sensing elements is called "voltage drop" and is not utilised to expand/contract the actuator [14]. It has been shown that charge estimators with a sensing resistor have the least voltage drop among all reported charge estimators of piezoelectric actuators [15]. Thus, these estimators were investigated and further developed in this research. Charge estimators of piezoelectric actuators with sensing resistor (CEPASRs) are widely called "digital charge estimators" [19], because, unlike other estimators, they cannot be implemented without digital processors. In this paper, instead of term 'digital', the acronym of CEPASR represents these estimators, as other estimators may be invented based on

digital technology in the future, or digital technology may be adopted to implement existing analogue charge estimators.

CEPASRs often use a fixed sensing resistor, e.g. [15, 20, 21]. In section III of this paper, it is manifestly shown that such estimators encounter either a significant voltage drop or impreciseness dealing with extensive operating areas. The observed dilemma was investigated, formulated and tackled.

II. CHARGE ESTIMATORS OF PIEZOELECTRIC ACTUATORS WITH SENSING RESISTOR (CEPASR)

Figure 1 is a schematic of a CEPASR. V_e is the 'excitation voltage'. V_S is the voltage across the sensing resistor, R_S, or the 'sensing voltage'. K_a is the voltage amplifier gain, and f_c is the cut-off frequency of the high-pass filter in Hz. The estimator includes (i) digital components, in a computer program or software, (ii) an I/O card incorporating digital to analogue (D/A) and analogue to digital (A/D) converters, and (iii) analogue components: the piezoelectric actuator, a sensing resistor and a voltage amplifier.

Since the sensing resistor, R_S, is grounded, the current passing the actuator, i_P, mostly proceeds through R_S, and only a minuscule current enters the analogue to digital converter, A/D in Fig 1. As a result, i_P is nearly equal to the current passing through R_S, i.e. i_R. Moreover, due to Kirchhoff voltage law, $V_S = i_R R_S$. Thus,
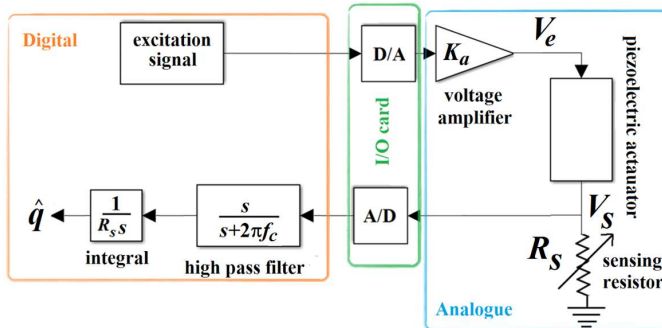
$$i_P \cong i_R = \frac{V_S}{R_S}. \tag{1}$$

Fig. 1. A schematic of the experimental setup used in this research

Integral of i_P equals the charge of the actuator; hence, theoretically, charge can be estimated through integration of $i_P = V_S / R_S$.

However, such an integration is tricky. A/D converters are not ideal and have a tiny offset voltage. This voltage alongside dielectric leakage of the piezoelectric actuator generate a low frequency (nearly constant) minute bias voltage, V_b. Therefore, the voltage of the current entering A/D is $V_S + V_b$, in practice. V_b is accumulated through integration and deviates estimation. That is, the estimated charge, $\hat{q}_P$, does not equal the actual charge of the actuator, q_P:

$$\hat{q}_P = \int \frac{V_S + V_b}{R_s} dt \neq \int \frac{V_S}{R_s} dt \cong q_P. \tag{2}$$

This discrepancy is called drift [21].The high-pass filter, shown in Fig.1, supresses low frequency V_b and avoids drift. However, this filter adversely suppresses low frequency

components of V_S too. Hence, a CEPASR of Fig.1 does not befit low frequency operating areas.

III. PROBLEM STATEMENT

In this work, CEPASRs were aimed to have (i) high precision and (ii) low voltage drop.

About the precision, A/D converter is a prominent role player. Every A/D convertor has a resolution (n bits) and one or a number of range(s) for input voltage. Then, in operation, 2^n digital numbers is assigned to the selected input range [22]. For instance, let us assume an A/D converter has a resolution of 10 bits, and input ranges of ± 0.5 V, ± 1 V and ± 5V. If the input range of ± 1 V is selected. 2^{10} numbers are assigned to the range of [-1 +1]V, or a digital number is assigned to 2V$/2^{10}$ or almost 1.95 mV of the input range. Evidently, if the input voltage (signal), covers a greater portion of the A/D input range, more digital numbers will be used to quantify the input signal. This leads to a higher precision. Therefore, with a known resolution, maximum precision is realised through full coverage of an A/D input range by the input signal, which is V_S in digital CEPASRs.

In terms of lowering the voltage, as to Fig.1, V_S is the voltage drop, the part of V_e not utilised for actuation. That is, V_S is targeted to be small.

As a result, for a given A/D, the following design guidelines can contribute to have both high precision and low voltage drop:

- V_S should fully cover an input range of the A/D.
- V_S should be small

Both these guidelines, with prioritising precision, can be merged as a design recommendation: V_S should fully cover the narrowest range of the A/D input voltage. This recommendation assures the highest precision at the lowest possible voltage drop.

With a known excitation voltage (depending on the desirable position profile) and A/D converter, R_S, in Fig. 1, is the sole variable to adjust V_S so as to fulfil the aforesaid design recommendation.

Figure 2 presents V_S for the estimator depicted in Fig.1.The actuator is a 5×5×36 mm³ piezoelectric stack of SA050536 type made by PiezoDrive [23], and R_S =44 Ω. The excitation voltage follows a triangular function with the peak to peak range of [0 20] V and frequencies of 20 Hz and 60 Hz. The narrowest input range of the A/D is ± 0.625 V. As to Fig.2, at the excitation frequency of 60 Hz, the input range is almost fully used, and the design recommendation is fulfilled. However, at the frequency of 20 Hz, 56% of input range is not used; thus, the guideline is not met.

Figure 2 shows that a CEPASR with a sole value of R_S cannot fulfil the recommendation in an extensive area of operation. Nevertheless, all reported digital charge estimators for piezo-actuators have either a single value [20, 21] or only a few intuitively selected values of R_S [15]. This research proposes an adaptive charge estimator with operation-condition-dependent R_S. Such a charge estimator needs a mathematical formula or model, F in (2 and 3), to approximate the appropriate R_S for any
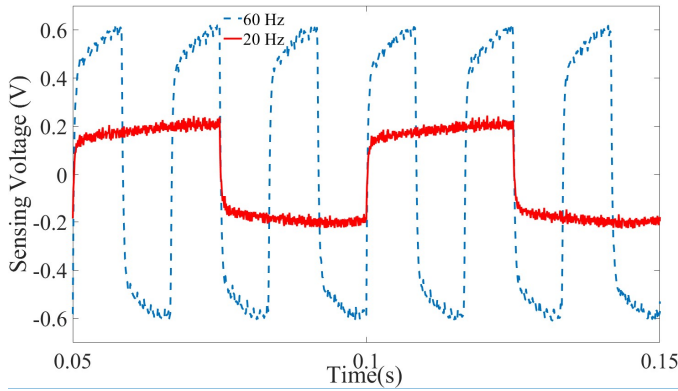
Fig. 2. The sensing voltage across the sensing resistor of 44 Ω with the excitation voltage range of 20 V at excitation frequencies of 20 Hz (red) and 60 Hz (blue). Tests were carried on piezoelectric stack actuators with dimensions of 5×5× 36 mm.

operating condition so as to satisfy the design recommendation:

$$\hat{R}_S = F(\text{operating conditions}), \qquad (2)$$

Operating conditions consist of amplitude and frequency of the excitation voltage (V_e in Fig.1) and its waveform. The symbol (^) refers to an approximated value.

This research merely concerns triangular excitation voltages. Because in scanning devices, one of the most common applications of nanopositioning, the actuator should track a triangular waveform [22]. Therefore, as waveform is known, the only operating conditions are the range, ρ, and frequency, f, of V_e:

$$\hat{R}_S = F(\rho, f). \qquad (3)$$

After $\hat{R}_S$ identification of F, (3) can adjust R_S to obtain an adaptive charge estimator. Sections V and VI present identification of F with approximate analytical models and fully connected cascade networks, respectively.

IV. EXPERIMENTATION

The experimental setup, an implementation of Fig.1, is shown in Fig.3. The digital processor is a personal computer with MATLAB 8. 6, Simulink 8.6 and Simulink Real-Time Desktop Toolbox 5.1 software. The actuator is a 5×5×36 mm³ piezoelectric stack made by PiezoDrive [23], and the amplifier is an AETECHRON 7114. The I/O card is an Advantech PCI-1710U with 12 bits of resolution of and five available A/D input ranges: ±10, ±5, ±2.5, ±1.25 and ±0.625 V.
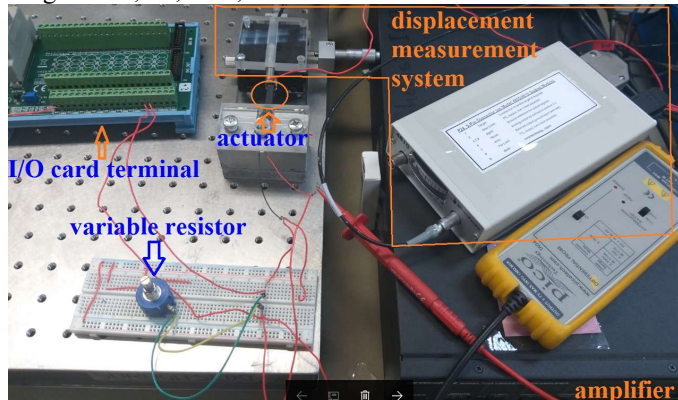

Fig. 3. Experimental setup, excluding the computer. Displacement sensor was not used in this research.

In order to develop/asses the function of F in (3), 35 experiments were conducted. In all of them, triangular excitation voltages with the minimum of zero and the range of ρ and the frequency of f were used:

$$V_e(t) = \begin{cases} 2\rho\left(tf - \text{truncate}(tf)\right) & \text{if } tf - \text{round}(tf) \geq 0, \\ -2\rho\left(tf - \text{truncate}(tf)\right) + 2\rho & \text{if } tf - \text{round}(tf) < 0. \end{cases} \qquad (4)$$

where t is time in seconds. In the collected experimental data, ρ and f have the values of 20, 30, 40, 50 or 60 V and 20, 30, 40, 50, 60, 70 or 80 Hz, respectively. In every experiment, R_S, was adjusted so that the sensing voltage touches the limits of [-0.625 +0.625] V, the narrowest voltage range of the A/D converter. That is, the value of R_S, with the best agreement to the recommendation, were experimentally found for each combination of excitation range and frequency. These results should ideally equal the outputs of F in (3) for different values of ρ and f.

V. ANALYTICAL APPROXIMATOR OF THE SENSING RESISTANCE

This section aims to analytically approximate F presented in (3) for voltage excitation of (4). For this purpose, the piezoelectric actuator is approximately considered as a capacitor, C_P [15]. Assuming that the current entering A/D is insignificant, the current passing the piezoelectric actuator i_P is presented in (6):

$$i_P(s) = \frac{V_e(s)}{R_S + \dfrac{1}{C_P s}} = \frac{V_S(s)}{R_S}. \qquad (5)$$

Due to (5), a linear relationship of (6) can be presented between V_S and V_e, (both shown Fig.1) [19]:

$$\frac{V_S(s)}{V_e(s)} = \frac{R_S C_P s}{R_S C_P s + 1}. \qquad (6)$$

Let us re-write (4) in the form of (7):

$$V_e(t) = \underbrace{\frac{\rho}{2}}_{\beta} + \overbrace{\begin{cases} 2\rho\left(tf - \text{truncate}(tf)\right) - \dfrac{\rho}{2} & \text{if } tf - \text{round}(tf) \geq 0, \\ -2\rho\left(tf - \text{truncate}(tf)\right)t + \dfrac{3\rho}{2} & \text{if } tf - \text{round}(tf) < 0. \end{cases}}^{V_{ewb}}$$

$$(7)$$

Then, V_{ewb} (bias-less excitation voltage) can be assumed as a triangular wave with the frequency of f Hz and the amplitude of 0.5ρ V, as depicted in Fig.4.

A. Analytical Model to Approximate the Sensing Resistance for a Bias-less Excitation Voltage

Bias-less excitation voltage can be presented as (8) using Fourier series:

$$V_{ewb}(t) = \frac{4\rho}{\pi^2} \sum_{n=0}^{\infty} \frac{-1}{(2n+1)^2} \sin\left((2n+1)2\pi ft + \frac{\pi}{2}\right) = \sum_{n=0}^{\infty} V_{es}(n,t),$$

$$(8)$$

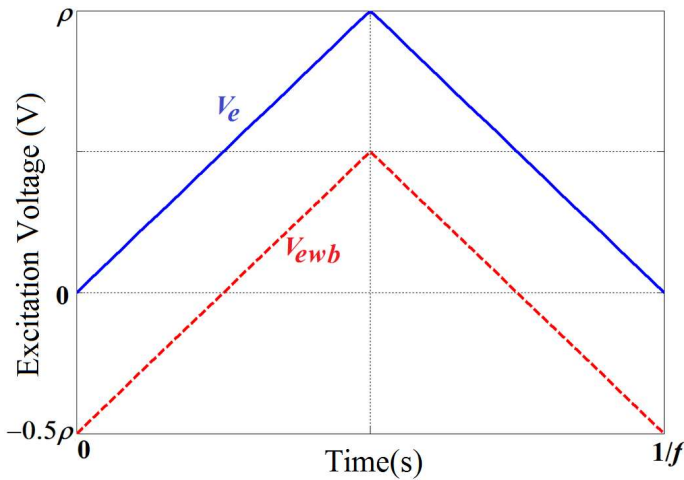where V_{es} is a sinusoidal constituent of V_e with the amplitude of

Fig. 4. Original (V_e) and bias-less (V_{ewb}) excitation voltages, described in (5) and (8)

$$A_{es}(n,t) = \frac{4\rho}{\pi^2} \frac{-1}{(2n+1)^2}. \tag{9}$$

As to the transfer function of (6), any excitation constituent of $V_{es}(n,t) = A_{es}(n,t)\sin\left((2n+1)2\pi ft + \frac{\pi}{2}\right)$ causes a sensing voltage constituent of

$$V_{Ss}(n,t) = A_{Ss}(n,t)\sin\left((2n+1)2\pi ft - \tan^{-1}(2\pi R_S C_P f) + \pi\right).$$

Considering (6) and (9),

$$A_{Ss}(n,t) = \left| \frac{R_S C_P j(2n+1)2\pi f}{R_S C_P j(2n+1)2\pi f + 1} \right| A_{es}(n,t)$$

$$= \frac{R_S C_P (2n+1)2\pi f}{\sqrt{(R_S C_P (2n+1)2\pi f)^2 + 1}} A_{es}(n,t) \tag{10}$$

$$\cong R_S C_P (2n+1)2\pi f \, A_{es}(n,t) = \frac{8\rho}{\pi} \frac{-1}{2n+1} R_S C_P f.$$

Due to linearity, presented in (6), superposition is usable:

$$V_S(t) = \sum_{n=1}^{\infty} V_{Ss}(n,t). \tag{11}$$

Considering (8), (10) and (11),

$$V_S \cong \frac{8\rho}{\pi} R_S C_P f \sum_{n=0}^{\infty} \frac{1}{2n+1} \sin\left((2n+1)2\pi ft - \tan^{-1}(2\pi R_S C_P f)\right), \tag{12}$$

Interestingly, (13) is the Fourier series of a square wave with the amplitude of A_S:

$$A_S \cong 2\rho R_S C_P f. \tag{13}$$

Thus, R_S leading to a sensing voltage amplitude of A_S, can be approximated as (15)

$$\hat{R}_S \cong \frac{A_S}{2\rho C_P f}. \tag{14}$$

In this paper, as detailed in sections III and IV, A_S=0.625 V and C_P =4.07 μF, then:

$$\hat{R}_S \cong \frac{7.678 \times 10^4}{\rho f}. \tag{15}$$

B. Effect of Bias

From (7), $V_e = V_{ewb} + \beta$. Based on superposition, two separate V_S constituents influenced by V_{ewb} and β (bias), respectively, may be added to result in V_S.

Let $V_{S\beta}$ be the constituent of V_S solely influenced by β. Using (6), (16) shows that the final value of $V_{S\beta}$ is zero:

$$\lim_{t \to \infty} V_{S\beta}(t) = \lim_{s \to 0} s V_{S\beta}(s) = \lim_{s \to 0} s \frac{R_S C_P s}{R_S C_P s + 1} \frac{\beta}{s} = 0. \tag{16}$$

As a result, the influence of the bias fades shortly, or the excitation bias (β) has no long lasting influence. Therefore, (14) and (15) are useable for excitations with a bias either.

VI. FCC NETWORK APPROXIMATOR OF THE SENSING RESISTANCE

In this research, a fully connected cascade (FCC) network of (18) was also employed to approximate F in (3). FCC network is a type of artificial neural networks (ANNs) with the most powerful architecture for system identification [24].

$$\hat{R}_S = \sum_{i=1}^{5} \mathbf{T}_i \phi\left(\mathbf{W}_{i1} f + \mathbf{W}_{i2} \rho + \mathbf{B}_i\right) + \mathbf{C}_1 f + \mathbf{C}_2 \rho + b, \tag{17}$$

where $\phi(\mathbf{x}) = \frac{2}{\exp(-2\mathbf{x}) - 1} - 1$. $\tag{18}$

Vectors/matrices $\mathbf{T}$, $\mathbf{W}$, $\mathbf{B}$ and $\mathbf{C}$ and scalar b are the parameters of this model, in total, 23 scalars or matrix/vector elements. Size of $\mathbf{T}$ (=5) was chosen based on the recommendations of [24], as the only difference of an FCC is with a multi-layer perceptron (e.g. the one introduced in [25, 26]) is $\mathbf{C}$ vector.

35 data sets of experimental data, detailed in section IV, were used to develop and validate the FCC model. 25, 5 and 5 randomly selected data sets were used to (i) identify model parameters, (ii) avoid overfitting and (iii) cross-validate the model. These data series, named modelling, validation and test data, were normalised prior to use, as explained in Appendix A.

The first step of parameter identification is parameter initialisation. Nguyen-Widrow method was employed for this purpose as introduced in Appendix B. Then, initial values of the parameters were tuned through an iterative algorithm (detailed in Appendix C) to minimise the modelling error. Modelling error was calculated with (19) (similar to the one in [27]) and the modelling data, n_d=25.

$$E = \frac{\sum_{i=1}^{n_d} \left(\hat{R}_{S_i} - R_{S_i}\right)^2}{n_d}. \tag{19}$$

where the value of R_{Si} and $\hat{R}_{Si}$ are obtained from experiments and (17), respectively. At each iteration, both modelling and validation errors were calculated. Validation error is the error calculated with (19) and 5 sets of validation data. Coincidence of decrease in the modelling error and increase in the validation error is a sign of overfitting and triggers to end parameter identification [28]. Overfitting diminishes the generality of ANNs [29, 30]. As explained in Appendix B, it is possible that the parameter identification algorithm is trapped and ends at a so-called local error minimum, i.e. an inaccurate model. Hence,
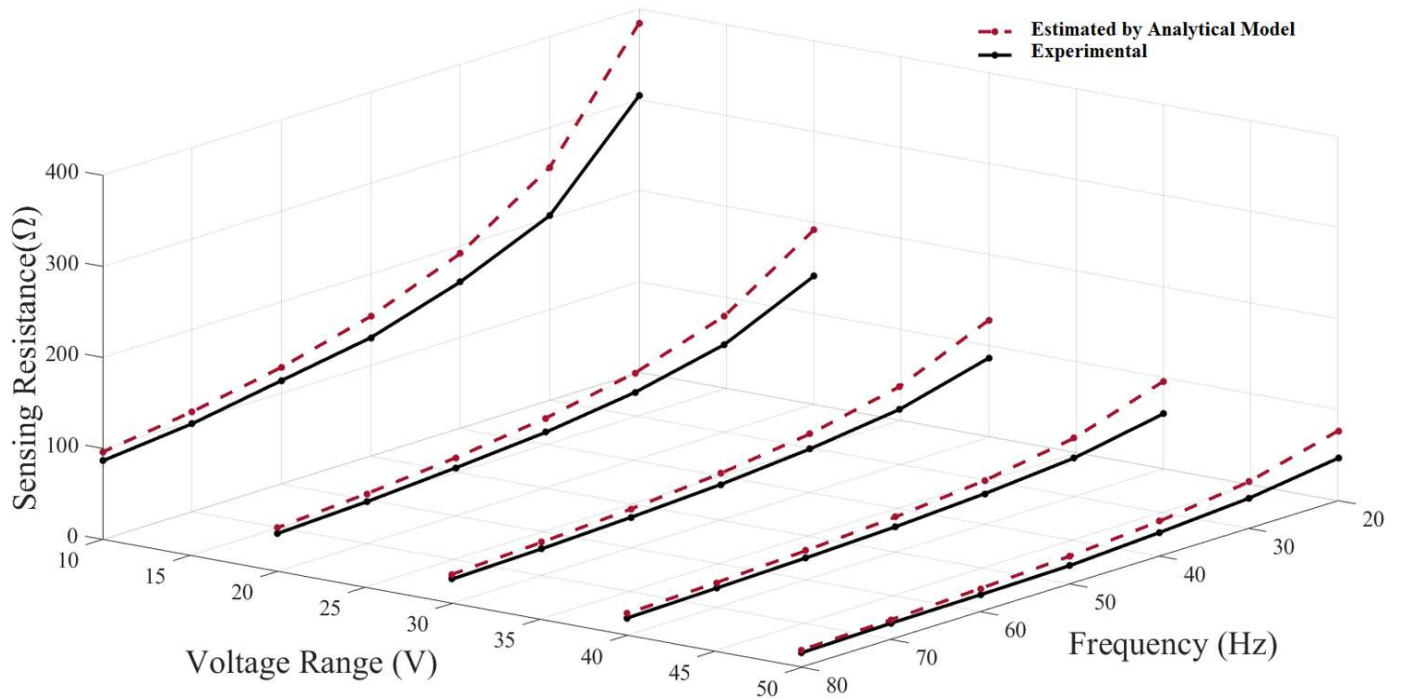
Fig. 5. Experimental versus analytically-estimated sensing resistances

parameter identification was repeated several times to assure about aptness of the model; the model with minimum validation error was opted.

After identifying model parameters, test error was calculated with (19) and the test data, used neither in parameter identification nor in overfitting avoidance. A reasonably small test error can ensure cross-validation [31].

VII. RESULTS AND DISCUSSION

This section first assesses the analytical model/approximator of the sensing resistance, then compares it with the developed FCC network. In the end, the risk of overestimation of R_S is discussed, and an alternative is presented to reduce this risk.

A. Analytical Model Results

Figure 5 compares the values of $\hat{R}_S$ approximated by the analytical model of (15) of section V with the experimental values of R_S. With use of R_S, V_S would fit into the narrowest input range of the A/D converter, i.e. [-0.625 0.625] V. The analytical model evidently overestimates the sensing resistance or $\hat{R}_S > R_S$. As a result, with use of $\hat{R}_S$, V_S would surpass A/D input range, as depicted in Fig. 6. Consequently, some values
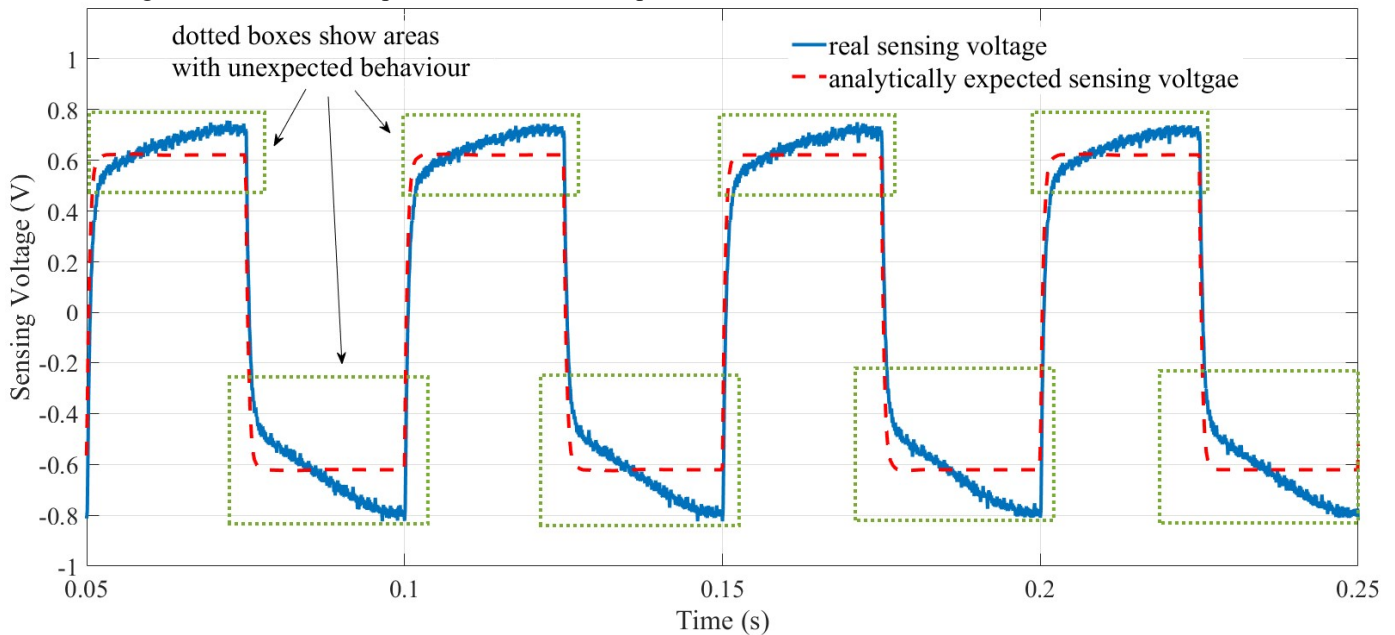

Fig. 6. The sensing voltage for excitation range (ρ) of 30 V and excitation frequency (f) of 20 Hz with the sensing resistance of 128 Ω, an output of (15) .

V_S would not be transferred to the computer and charge estimation would be interrupted. Therefore, analytically approximated values of the sensing resistor should not be used in practice. Figure 6 clearly demonstrates that the analytical approximate model cannot explain the behaviour of the actuator in full.

For the entire available data, the mean absolute value of error from the analytical model is 19.26 Ω, 6.33% of maximum R_S. Relative error, $(\hat{R}_S - R_S)/R_S$ (20), varies between 11.21% to 64.41%. Relative error increases with decrease of excitation frequency and increase of excitation voltage range (ρ). The approximation bias, Б, average of $(\hat{R}_S - R_S)$ is 19.26 Ω, equal to the mean absolute value of error, because $\hat{R}_S > R_S$ in all operating conditions. Standard deviation, σ, of approximation by the analytical model is 14.96 Ω.

B. Comparison of Analytical Model and FCC Network

Table 1 and Fig.7 compare the outputs of the FCC network developed in section VI, a combination of (17) and (18), and the analytical model. The aforesaid table and figure only include five test data sets; as other 30 data sets have been used in development of the FCC network and match to this model extremely well.
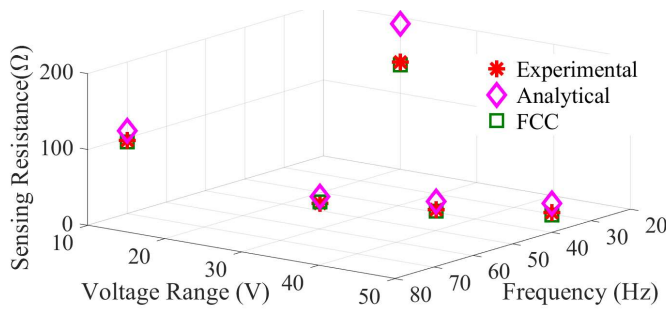

Fig. 7. The values of the sensing resistance for the test data, experimental values and approximated values by different models

The FCC network obviously outperforms the analytical model. For the test data, mean absolute value of error for the analytical model and the FCC network are 19.26 Ω (accidentally same as the one for the entire data) and 2.49 Ω, respectively. The approximation bias for the analytical model and the FCC network are 19.26 Ω and -1.81 Ω. Standard deviation of approximation by the analytical model and the FCC network are 15.81 Ω and 1.95 Ω, respectively.

C. Overestimation Avoidance

As detailed in section III and subsection VII.A, overestimation of the sensing resistor has a seriously damaging consequence, i.e. saturation of V_S (loss of V_S data at times). However, underestimation of R_S only results in the decrease of precision, because it causes the range of V_S to be narrower than the narrowest input range of the A/D converter. The developed FCC network has a negative approximation bias. That is, it advantageously tends to underestimate the sensing resistor not to overestimate them.

Assuming $(\hat{R}_S - R_S)$ has a Gaussian distribution, there is 50% chance of overestimation for any unbiased approximator (with Б =0) [32]. (21) is suggested to avoid overestimation of the sensing resistance (leading to saturation of V_S).

$$\hat{R}_{SP} = \hat{R}_S - Б - 3\sigma, \tag{21}$$

where $\hat{R}_{SP}$ is practical approximated sensing resistance. According to [32], use of $\hat{R}_{SP}$ reduces the chance of overestimation of the sensing resistance to 1%.

TABLE I
SENSING RESISTANCE APPROXIMATION RESULTS FOR THE ANALYTICAL
MODEL AND THE FCC NETWORK

ρ (V)	f (Hz)	R_S	$\hat{R}_S$		Relative Error%	
			Analytical	FCC Net	Analytical	FCC Net
10	70	96.5	109.7	94.8	13.7	-1.9
20	20	141.2	192.0	137.3	36.0	-2.8
30	60	33.5	42.7	35.2	27.3	5.0
40	50	27.6	38.4	25.9	39.1	-6.1
50	40	26.0	38.4	22.6	47.7	-13.1

VIII. CONCLUSION

The paper first briefly introduced charge estimators of piezoelectric actuators with a sensing resistor (CEPASRs) in section II. Then, CESPARs' design aiming at maximum estimation accuracy with the smallest possible voltage drop guideline was investigated. This investigation led to a practical design recommendation. The only adjustable parameter of a CEPASR is its sensing resistance, R_S. Reported experimental results show that a sole value of the sensing resistance cannot fulfil the design recommendation for an extensive operating area. This observation justifies the use of an adaptive R_S. Considering the fact that reported CEPASRs (and other charge estimators) in the literature normally use a single or a few values of R_S (or other sensing elements) shows the significance of this paper's results.

A CEPASR with an adaptive sensing resistance needs a formula to suggest R_S for different operating conditions. Two approaches were adopted to tackle this task: (1) analytical modelling and formulation, with the assumption that a piezoelectric actuator electrically behaves similar to a capacitor, and (2) development and use of a fully connected cascade (FCC) network, a type of artificial neural network. The latter presented much more accurate estimation. FCC network's mean of absolute test error is 2.49 Ω which is nearly 8 times smaller than the one of the analytical model. Interestingly, analytical approach led to a positive bias, i.e. overestimation of R_S, in all operating conditions.

It was discussed that an overestimated R_S leads to saturation of the sensing voltage and loss of charge data for some time spans ; while, underestimation of R_S only leads to loss in estimation precision to some extent. Even an ideal unbiased model has a 50% chance of overestimation; thus, a formula, (22), was developed and suggested to decrease this chance to only 1% at the cost of higher chance of underestimation.

APPENDIX A. DATA NORMALISATION

Prior to use of data for any task in model development, the

input and output data columns are regularly normalised to eliminate the influence of magnitude discrepancy between variables [33]. As a customary method of normalisation, in this research, the data were mapped from their actual range into the range of [-1 1]. After model development with the normalised data, to employ the model, the input data to the model need to be normalised (mapped to the range of [-1 1]) and the output(s) of the model need to be de-normalised (de-mapped) into the actual range. Normalisation and de-normalisation may be integrated into the algorithms of development and use of the models [28].

APPENDIX B. BRIEF INTRODUCTION TO NGUYEN-WIDROW WEIGHT INITIALISATION ALGORITHM

The employed FCC network has a sigmoid function of $\phi(\cdot)$, introduced in (18). As depicted in Fig.B.1, a sigmoid function is almost linear for an interval. Outer this interval, the output is nearly saturated or constant. As a result, an input to $\phi(\cdot)$, located outside the linear interval, only has a trivial effect on the output, the error (as defined in (20)) and modelling process. Such a situation results in a sluggish parameter identification process. Nguyen-Widrow algorithm suggests initial values for elements of **W** and **B** (in 18) so that the input to $\phi(\cdot)$ lies within its linear interval [34, 35], as the first major advantage of this algorithm.

Parameter identification algorithm of this research, and all derivative-based optimisation algorithms, may be trapped in a local minimum [36]. Therefore, these algorithms may not yield the absolute minimum error function at every single attempt. If such algorithms restart from the same initial values of parameters, they move towards the same trap again. Nguyen-Widrow parameter initialisation algorithm includes random functions to change initial parameters at every attempt and avoid the aforementioned issue. This is the second major advantage of Nguyen-Widrow parameter initialisation algorithm.
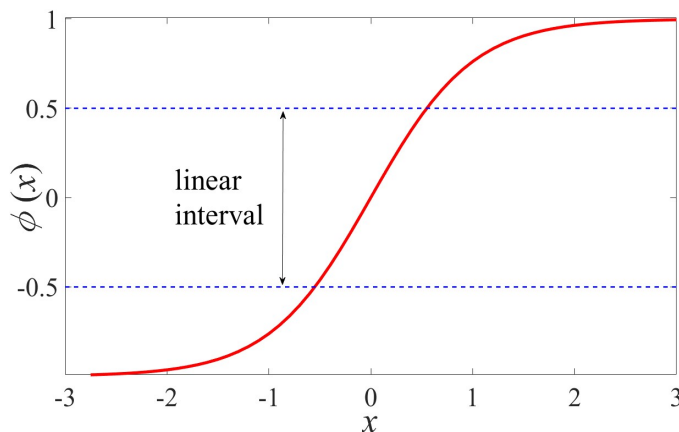

Figure B.1. The sigmoid function of (18) and its linear interval

APPENDIX C. PARAMETER IDENTIFICATION ALGORITHM

In order to explore the parameter identification algorithm, let us present E , defined in (19), as $E(\boldsymbol{\theta})$, where $\boldsymbol{\theta}$ is a vector of all 23 parameters of the FCC network. An iterative parameter

identification often adjusts $\boldsymbol{\theta}$ elements (from their initial values) so as to minimise $E(\boldsymbol{\theta})$.

A popular approach to reach a parameter adjustment algorithm is to approximate $E(\boldsymbol{\theta})$ with Taylor series up to the second order derivatives:

$$E(\boldsymbol{\theta} + \Delta\boldsymbol{\theta}) \cong E(\boldsymbol{\theta}) + \frac{\partial E(\boldsymbol{\theta})}{\partial \boldsymbol{\theta}}(\Delta\boldsymbol{\theta}) + \frac{1}{2}\frac{\partial^2 E(\boldsymbol{\theta})}{\partial \boldsymbol{\theta}^2}(\Delta\boldsymbol{\theta})^2. \qquad (C.1)$$

The following are the derivatives of $\boldsymbol{\theta}$ vector:

$$\frac{\partial E(\boldsymbol{\theta})}{\partial \boldsymbol{\theta}} = \mathbf{g} = \left[\frac{\partial E(\boldsymbol{\theta})}{\partial \theta_1}, \cdots, \frac{\partial E(\boldsymbol{\theta})}{\partial \theta_{n_p}} \right]^T.$$

$$\frac{\partial^2 E(\boldsymbol{\theta})}{\partial \boldsymbol{\theta}^2} = \mathbf{H} = \begin{bmatrix} \frac{\partial^2 E(\boldsymbol{\theta})}{\partial \theta_1^2} & \frac{\partial^2 E(\boldsymbol{\theta})}{\partial \theta_1 \partial \theta_2} & \cdots & \frac{\partial^2 E(\boldsymbol{\theta})}{\partial \theta_1 \partial \theta_{n_p-1}} & \frac{\partial^2 E(\boldsymbol{\theta})}{\partial \theta_1 \partial \theta_{n_p}} \\ \vdots & & \ddots & & \vdots \\ \frac{\partial^2 E(\boldsymbol{\theta})}{\partial \theta_{n_p} \partial \theta_1} & \frac{\partial^2 E(\boldsymbol{\theta})}{\partial \theta_{n_p} \partial \theta_2} & \cdots & \frac{\partial^2 E(\boldsymbol{\theta})}{\partial \theta_{n_p} \partial \theta_{n_p-1}} & \frac{\partial^2 E(\boldsymbol{\theta})}{\partial \theta_{n_p}^2} \end{bmatrix},$$

where n_p is the number of parameters.

As a result of (C.1), Newton direction, presented in (C.2), can theoretically minimise $E(\boldsymbol{\theta})$ [37]:

$$\Delta\boldsymbol{\theta} = -\mathbf{H}^{-1}\mathbf{g}. \qquad (C.2)$$

Nevertheless, if $\mathbf{H}$ is not invertible, (C.2) is no longer useable. Alternatively, Levenberg and Marquardt [37] proposed (C.3) to fix this shortcoming and generalise (C.2):

$$\Delta\boldsymbol{\theta} = -\eta\,(\mathbf{H} + \lambda\,\mathbf{I})^{-1}\mathbf{g}. \qquad (C.3)$$

where $\mathbf{I}$ is the identity matrix with the dimension of $n_p{\times}n_p$, λ is the smallest value that can make $\mathbf{H}+\lambda\mathbf{I}$ invertible. After finding λ, the value of η is computed with linear search. Further details on finding η and λ are available in[37, 38].

REFERENCES

[1] X. Li and C. Cheah, "Robotic cell manipulation using optical tweezers with unknown trapping stiffness and limited FOV," IEEE/ASME Transactions on Mechatronics, vol. 20,no.4,pp. 1624-1632, 2015.

[2] G. M. Clayton, S. Tien, K. K. Leang, Q. Zou, and S. Devasia, "A review of feedforward control approaches in nanopositioning for high-speed SPM," Journal of Dynamic Systems, Measurement, and Control, vol. 131,no.,pp. 061101, 2009.

[3] Y. H. Teh, "Labview Based Pid Algorithm Development for Z Motion Control in Atomic Force Microscopy," UTAR, 2015.

[4] H. Tang, Z. Zeng, J. Gao, and X. Zhang, "A flexible parallel nanopositioner for large-stroke micro/nano machining," in *International Conference on Manipulation, Manufacturing and Measurement on the Nanoscale (3M-NANO)*, 2015, pp. 107-110.

[5] S. Saedi, A. Mirbagheri, A. Jafari, and F. Farahmand, "A local hybrid actuator for robotic surgery instruments," International Journal of Biomechatronics and Biomedical Robotics vol. 3,no.2,pp. 100-105, 2014.

[6] M. Ghodsi, A. Saleem, A. Özer, I. Bahadur, K. Alam, A. Al-Yahmadi*, et al.*, "Elimination of thermal instability in precise positioning of Galfenol actuators," in *Behavior and Mechanics of Multifunctional Materials and Composites* 2016, p. 980008.

[7] V. Protopopov, "Beam Alignment and Positioning Techniques," in *Practical Opto-Electronics*, ed: Springer, 2014, pp. 309-334.

[8] L. Díaz Pérez, M. Torralba Gracia, J. Albajez García, and J. Yagüe Fabra, "One-Dimensional Control System for a Linear Motor of a Two-Dimensional Nanopositioning Stage Using Commercial Control Hardware," Micromachines, vol. 9,no.9,pp. 421, 2018.

[9] M. Mohammadzaheri and A. AlQallaf, "Nanopositioning systems with piezoelectric actuators, current state and future perspective," Science of Advanced Materials, vol. 9,no.7,pp. 1071-1080, 2017.

[10] S. O. R. Moheimani, "Invited Review Article: Accurate and fast nanopositioning with piezoelectric tube scanners: Emerging trends and future challenges," Review of Scientific Instruments, vol. 79,no.7,pp. 071101, 2008.

[11] N. Miri, M. Mohammadzaheri, and L. Chen, "An enhanced physics-based model to estimate the displacement of piezoelectric actuators," Journal of Intelligent Material Systems and Structures, vol. 26,no.11,pp. 1442-1451, 2015.

[12] K. A. Yi and R. J. Veillette, "A charge controller for linear operation of a piezoelectric stack actuator," IEEE Transactions on Control Systems Technology, vol. 13,no.4,pp. 517-526, 2005.

[13] M. Bazghaleh, S. Grainger, B. Cazzolato, and T.-f. Lu, "An innovative digital charge amplifier to reduce hysteresis in piezoelectric actuators," presented at the Australian Robotics and Automation Association (ACRA), Brisbane, Australia, 2010.

[14] J. Minase, T. F. Lu, B. Cazzolato, and S. Grainger, "A review, supported by experimental results, of voltage, charge and capacitor insertion method for driving piezoelectric actuators," Precision Engineering, vol. 34,no.4,pp. 692-700, 2010.

[15] M. Bazghaleh, S. Grainger, M. Mohammadzaheri, B. Cazzolato, and T. Lu, "A digital charge amplifier for hysteresis elimination in piezoelectric actuators," Smart Materials and Structures, vol. 22,no.7,pp. 075016, 2013.

[16] C. Yang, C. Li, and J. Zhao, "A Nonlinear Charge Controller With Tunable Precision for Highly Linear Operation of Piezoelectric Stack Actuators," IEEE Transactions on Industrial Electronics, vol. 64,no.11,pp. 8618-8625, 2017.

[17] S.-T. Liu, J.-Y. Yen, and F.-C. Wang, "Compensation for the Residual Error of the Voltage Drive of the Charge Control of a Piezoelectric Actuator," Journal of Dynamic Systems, Measurement, and Control, vol. 140,no.7,pp. 1-9, 2018.

[18] M. Bazghaleh, S. Grainger, M. J. J. o. I. M. S. Mohammadzaheri, and Structures, "A review of charge methods for driving piezoelectric actuators," Journal of Intelligent Material Systems and Structures, vol. 29,no.10,pp. 2096-2104, 2018.

[19] M. Mohammadzaheri, M. Emadi, M. Ghodsi, E. Jamshidi, I. Bahadur, A. Saleem, *et al.*, "A variable-resistance digital charge estimator for piezoelectric actuators: An alternative to maximise accuracy and curb voltage drop," Journal of Intelligent Material Systems and Structures, vol. 30,no.11,pp. 1699-1705, 2019.

[20] M. Bazghaleh, S. Grainger, M. Mohammadzaheri, B. Cazzolato, and T.-F. Lu, "A novel digital charge-based displacement estimator for sensorless control of a grounded-load piezoelectric tube actuator," Sensors and Actuators A: Physical, vol. 198,no.,pp. 91-98, 2013.

[21] M. Bazghaleh, M. Mohammadzaheri, S. Grainger, B. Cazzolato, and T. F. Lu, "A new hybrid method for sensorless control of piezoelectric actuators," Sensors and Actuators A: Physical, vol. 194,no.,pp. 25-30, 2013.

[22] M. Mohammadzaheri, S. Grainger, and M. Bazghaleh, "A system identification approach to the characterization and control of a piezoelectric tube actuator," Smart Materials and Structures, vol. 22,no.10,pp. 105022, 2013.

[23] PiezoDrive. (2018). *PiezoDrive Products*. Available: https://www.piezodrive.com/

[24] D. Hunter, H. Yu, M. S. Pukish III, J. Kolbusz, and B. M. Wilamowski, "Selection of proper neural network sizes and architectures—A comparative study," IEEE Transactions on Industrial Informatics, vol. 8,no.2,pp. 228-240, 2012.

[25] M. Mohamadian, H. Afarideh, and F. Babapour, "New 2d matrix-based neural network for image processing applications," IAENG International Journal of Computer Science, vol. 42,no.3,pp. 265-274, 2015.

[26] M. A. Aslam, C. Xue, M. Liu, K. Wang, and D. Cui, "Classification and Prediction of Gastric Cancer from Saliva Diagnosis using Artificial Neural Network," Engineering Letters, vol. 29,no.1,pp. 10-24, 2021.

[27] Z. Berradi, M. Lazaar, H. Omara, and O. Mahboub, "Effect of Architecture in Recurrent Neural Network Applied on the Prediction of Stock Price," IAENG International Journal of Computer Science, vol. 47,no.3,pp. 436-441, 2020.

[28] M. Mohammadzaheri, R. Tafreshi, Z. Khan, M. Ghodsi, M. Franchek, and K. Grigoriadis, "Modelling of petroleum multiphase flow in electrical submersible pumps with shallow artificial neural networks," Ships and Offshore Structures,pp. 1-10, 2019.

[29] M. Mohammadzaheri, A. Mirsepahi, O. Asef-Afshar, and H. Koohi, "Neuro-fuzzy modeling of superheating system of a steam power plant," Applied Math. Sci, vol. 1,no.,pp. 2091-2099, 2007.

[30] G. C. Cawley and N. L. Talbot, "On over-fitting in model selection and subsequent selection bias in performance evaluation," Journal of Machine Learning Research, vol. 11,no.Jul,pp. 2079-2107, 2010.

[31] A. Lendasse, V. Wertz, and M. Verleysen, "Model selection with cross-validations and bootstraps—application to time series prediction with RBFN models," Artificial Neural Networks and Neural Information Processing—ICANN/ICONIP 2003,pp. 174-174, 2003.

[32] D. C. Montgomery and G. C. Runger, *Applied statistics and probability for engineers*: John Wiley and Sons, 2014.

[33] M. Mohammadzaheri and L. Chen, "Intelligent Modelling of MIMO Nonlinear Dynamic Process Plants for Predictive Control Purposes," in *The 17th World Congress of The International Federation of Automatic Control*, Seoul, Korea, 2008, pp. 12401-12406.

[34] M. Mohammadzaheri, R. Tafreshi, Z. Khan, M. Franchek, and K. Grigoriadis, "An intelligent approach to optimize multiphase subsea oil fields lifted by electrical submersible pumps," Journal of Computational Science, vol. 15,no.,pp. 50-59, 2016.

[35] D. Nguyen and B. Widrow, "Improving the learning speed of 2-layer neural networks by choosing initial values of the adaptive weights," presented at the International Joint Conference on Neural Networks, San Diego, USA., 1990.

[36] M. Mohammadzaheri, L. Chen, A. Ghaffari, and J. Willison, "A combination of linear and nonlinear activation functions in neural networks for modeling a de-superheater," Simulation Modelling Practice and Theory, vol. 17,no.2,pp. 398-407, 2009.

[37] J. R. Jang, C. Sun, and E. Mizutani, *Neuro-Fuzzy and Soft Computing*. New Delhi: Prentice-Hall of India, 2006.

[38] M. Mohammadzaheri and L. Chen, "Intelliegnt Predictive Control of Model Helicopters' Yaw Angle," Asian Journal of Control, vol. 12,no.6,pp. 1-13, 2010.